Intrinsic Point-Defect Balance in Self-Ion-Implanted ZnO

Pekka T. Neuvonen,[1,2,*] Lasse Vines,[1] Bengt G. Svensson,[1] and Andrej Yu. Kuznetsov[1]

[1]*Department of Physics, Centre for Material Science and Nanotechnology, University of Oslo, P.O. Box 1048 Blindern, N-0316 Oslo, Norway*

[2]*Department of Physics and Astronomy, University of Aarhus, Ny Munkegade 120, 8000 Aarhus C, Denmark*

(Received 16 July 2012; published 3 January 2013)

The role of excess intrinsic atoms for residual point defect balance has been discriminated by implanting Zn or O ions into Li-containing ZnO and monitoring Li redistribution and electrical resistivity after postimplant anneals. Strongly Li-depleted regions were detected in the Zn-implanted samples at depths beyond the projected range (R_p) upon annealing $\geq 600\,^{\circ}\mathrm{C}$, correlating with a resistivity decrease. In contrast, similar anneals of the O-implanted samples resulted in Li accumulation at R_p and an increased resistivity. Control samples implanted with Ar or Ne ions, yielding similar defect production as for the Zn or O implants but with no surplus of intrinsic atoms, revealed no Li depletion. Thus, the depletion of Li shows evidence of excess Zn interstitials (Zn_I) being released during annealing of the Zn-implanted samples. These Zn_I's convert substitutional Li atoms ($\mathrm{Li}_{\mathrm{Zn}}$) into highly mobile interstitial ones leading to the strongly Li-depleted regions. In the O-implanted samples, the high resistivity provides evidence of stable O_I-related acceptors.

DOI: 10.1103/PhysRevLett.110.015501 PACS numbers: 81.05.Dz, 72.80.Ey, 66.30.Lw, 71.55.Gs

Zinc oxide (ZnO) is a promising material for optoelectronic and sensor applications. Indeed, it has a wide and direct band gap ($E_g \simeq 3.4$ eV), suitable for UV or white light sensors or sources, as well as a high exciton binding energy (~60 meV) [1], enabling, for instance, efficient lasing at room temperature (RT). Selective area doping by ion implantation is an important technology for a successful implementation of such devices, but it may also be used as a tool to understand intrinsic point defects when monitoring the evolution of the radiation damage. Previous ion-implantation or -irradiation studies of ZnO have shown that a significant fraction of the induced disorder disappears already at RT, making ZnO a remarkably radiation hard material [2–5]. Specifically, Zn interstitials (Zn_I) were suggested to be mobile even at temperatures below RT, so that the recombination with Zn vacancies (V_{Zn}) is prominent during bombardment [4]. However, in spite of the high dynamic annealing rates, residual disorder remains in the Zn sublattice as well as in the oxygen sublattice (oxygen vacancies, V_{O}, and interstitials, O_I) and, in principle, also antisite defects may form. Notably, it is challenging to discriminate between individual contributions of these intrinsic and fundamental point defects and a common interpretation is often made in terms of an overall implantation induced disorder [5], usually measured by Rutherford backscattering spectrometry. In its turn, chemical profiling, which is highly suitable to study impurities and diffusion, has a limited applicability because intrinsic defects are obviously indistinguishable from substitutional matrix atoms.

Among the growth techniques used for ZnO, the hydrothermal (HT) method is appreciated for its potential scalability to produce good quality, single crystalline wafers [6]. However, a high Li content in HT ZnO is an issue of concern and postgrowth treatment is required for its reduction [7,8]; especially, Li exhibits a so-called amphoteric behavior resulting in highly compensated material [9,10]. In as-grown HT ZnO, Li resides predominantly on Zn site [9], forming $\mathrm{Li}_{\mathrm{Zn}}$ acceptors, but can be potentially kicked out to an interstitial donor position (Li_I) during, for instance, postimplantation anneals [11]. Accordingly, HT ZnO, naturally containing $\sim 2 \times 10^{17}$ $\mathrm{Li/cm^3}$, is a suitable model system to identify dominating residual point defects involved in the $\mathrm{Li}_{\mathrm{Zn}}$ kick-out mechanism. Indeed, intriguing Li redistribution in the form of ''depletion'' or ''pile-up'' after postimplant annealing have been reported previously in the literature [12] but with a limited understanding.

In order to discriminate between the roles of different kinds of intrinsic defects in ZnO, we have performed self-ion implants and, exploiting the high dynamic annealing rate, an excess of the corresponding interstitial defects is anticipated during postimplant heat treatment with the ultimate limit equal to the ion dose. Combining Li chemical profiling with resistivity measurements, we find convincing evidence for Li depletion caused by excess of Zn_I, readily kicking out $\mathrm{Li}_{\mathrm{Zn}}$, while a surplus of O_I causes electrical compensation and no Li-depletion.

10×10 $\mathrm{mm^2}$ HT ZnO wafers [c-axis oriented, $(000\bar{1})$] having an initial resistivity (ρ) and Li concentration in the range of 0.1–0.5 $\mathrm{k\Omega\,cm}$ and $2\text{–}4 \times 10^{17}$ $\mathrm{cm^{-3}}$, respectively, were used. Excess intrinsic atoms (presumably residing as surplus interstitials) were introduced either by O or Zn ion implants. In order to discriminate between these surplus interstitials and those generated in the course of elastic energy deposition (damage formation), Ne or Ar

ion implants were performed with energy and fluence parameters yielding similar disorder profiles as for the O or Zn ions, respectively, according to Monte Carlo simulations [13–15]. These control experiments were performed with a so-called "high" fluence ($\sim 10^{16}$ ions/cm^2) and the corresponding samples were labeled as H_Zn, H_Ar, H_Ox, and H_Ne. In addition, 2 orders of magnitude lower fluence (a so-called "low" fluence and samples labeled as L_Zn and L_Ox) was also used to investigate possible concentration effects for the surplus of self-interstitials. All the implants were performed at RT with fluxes of $\sim 10^{12}$ cm^{-2} s^{-1}. Further, the wafers were cut into pieces with a typical size of 5×5 mm^2, which were subjected to anneals at 600, 800, or 1000 °C for 1 h in air using a conventional tube furnace. One piece of the H_Zn wafer was isochronally (30 min) annealed from 550 to 850 °C (steps of 25–50 °C) in air while another piece was isothermally annealed at 800 °C in air for durations of 1–318 s using a rapid thermal processing furnace (50 °C/s heating ramp and ~100 °C/s cooling ramp).

Li concentration versus depth profiles were measured by secondary ion mass spectrometry (SIMS) employing a Cameca IMS7f microanalyzer. A beam of 10 keV O_2^+ ions was rastered over a surface area of 125×125 μm^2 and secondary ions were collected from the central part of the sputtered crater. Crater depths were measured with a Dektak 8 stylus profilometer, and a constant erosion rate was assumed when converting sputtering time to sample depth. Calibration of the Li signal was performed using an implanted reference sample and the detection limit was in the low 10^{14} cm^{-3} range.

After the SIMS measurements, the samples were cleaved with cross sections (edges) such that electrical resistance profiles could be determined employing a VEECO D3100 atomic force microscope operated in scanning spreading resistance mode (SSRM). A conductive Ti-Pt covered silicon tip was used in contact mode and a DC bias voltage was applied between the sample and the tip. The back side contact was obtained by wrapping the samples in a conductive Cu tape with a droplet of eutectic indium-gallium in between. Generally, SSRM data are of limited quantitative validity but sufficiently accurate for qualitative conclusions. The as-grown samples revealed typically flat SSRM signals in the range of 10^8 Ω while the as-implanted samples were highly resistive and out of range.

Figures 1(a) and 1(b) show Li concentration and SSRM signal versus depth profiles for the L_Zn, H_Zn, and H_Ar samples. In the L_Zn sample, the 600 °C annealing does not affect the Li distribution dramatically while 800 °C results in a decreasing concentration at depths up to ~1 μm beyond R_p ($R_p \approx 180$ nm). In contrast, for the H_Zn sample a substantial Li depletion occurs already after the 600 °C anneal. Spectacularly, 800 °C gives a rise to a depleted region of at least 5.5 μm beyond R_p,

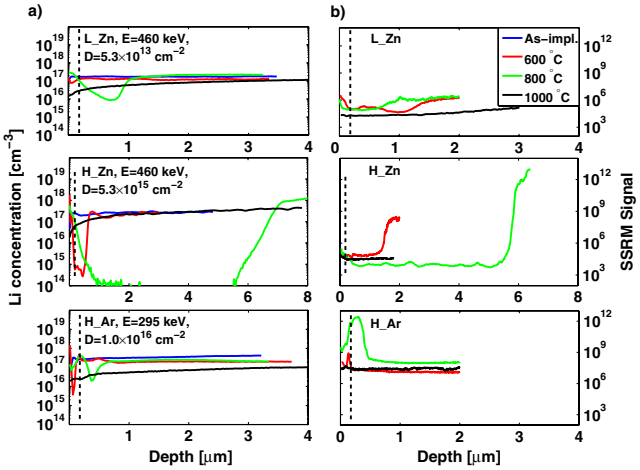

FIG. 1 (color online). (a) Li concentration versus depth profiles measured by SIMS and (b) corresponding SSRM signals for Zn- and Ar-ion-implanted samples. The annealing time was 1 h for all the temperatures. The dashed lines indicate R_p of the implanted ions (~180 nm). Notice the difference in depth scale for sample H_Zn due to the deep Li redistribution.

and the residual Li concentration is below the detection limit. These results alone suggest that Li redistribution is promoted by intrinsic defects because of the pronounced fluence dependence. However, the question on the origin of defects mediating Li redistribution remains, and corresponding Ar implants were undertaken. As illustrated in the lower panel of Fig. 1(a), no broad Li-depleted region appears in the H_Ar samples after 600 and 800 °C, but, instead, some accumulation occurs around R_p (surrounded by two narrow Li-lean regions). In general, the overall magnitude of Li redistribution at 600 and 800 °C is minor in the H_Ar samples compared to that in the H_Zn samples. After 1000 °C, all samples in Fig. 1(a) exhibit rather similar profiles suggesting a substantial removal of the implantation induced defects and minor effect on the Li outdiffusion.

Figure 1(b) reveals a clear resemblance of the SSRM profiles with the SIMS profiles in Fig. 1(a). This is most pronounced for the H_Zn samples annealed at 800 °C, where the Li-depleted region exhibits a low resistivity as unveiled by the abrupt and large step in the SSRM signal. Upon 600 °C annealing, H_Zn reveals a low resistive region extending slightly deeper than the Li-depleted one, and a close examination of the Li profile shows a buildup beyond the depleted layer. This may indicate that a fraction of the redistributed Li atoms reside as donors (Li_I) in this region. Consistent with the minor Li redistribution in the L_Zn samples, the SSRM signal also displays only small variations, with a weak indication of a plateau having an extension close to that of the Li-depleted region after 800 °C. In the H_Ar samples, the SSRM signals are in direct contrast to those in the H_Zn samples with a strong increase around R_p and no existence of a low-resistivity

region. Accordingly, combining the SIMS and SSRM results in Fig. 1, we may conclude that the presence of Zn_I's plays a decisive role; a surplus of Zn_I's converts less mobile Li_{Zn} acceptors to highly mobile Li_I donors resulting in Li-depleted n-type regions with a low resistivity [16].

Figures 2(a) and 2(b) show the Li concentration and SSRM signal versus depth for the L_Ox, H_Ox, and H_Ne samples. Comparing the Li redistribution in the L_Ox and H_Ox samples, a distinct fluence dependence of the amount of Li accumulated around R_p upon annealing at 600 and 800 °C is observed. Further, in direct contrast to the Zn-implanted samples, no depletion of Li occurs beyond R_p. The results for the control H_Ne sample confirm that it is not the displacement of matrix atoms but again the surplus of implanted self-ions (oxygen) that governs the Li redistribution. Note upon the 600 and 800 °C anneals, the H_Ne and H_Ar samples display rather similar Li profiles but with some difference in absolute magnitude, presumably caused by the difference in defect production rates between the two ions [17]. In accordance with the data in Fig. 1(a), all samples in Fig. 2(a) annealed at 1000 °C also show Li profiles having characteristic "outdiffusion" tails toward the surface.

The resistance evolution in the H_Ne samples after 600 and 800 °C, Fig. 2(b), is almost identical to that in the H_Ar samples, Fig. 1(b), with a peak around R_p while deeper regions are more conductive. However, after 1000 °C, the resistance of the H_Ne sample resembles that of the L_Zn and H_Zn samples, while the H_Ar sample exhibits a substantially higher value, as also confirmed by four-point-probe measurements. This may

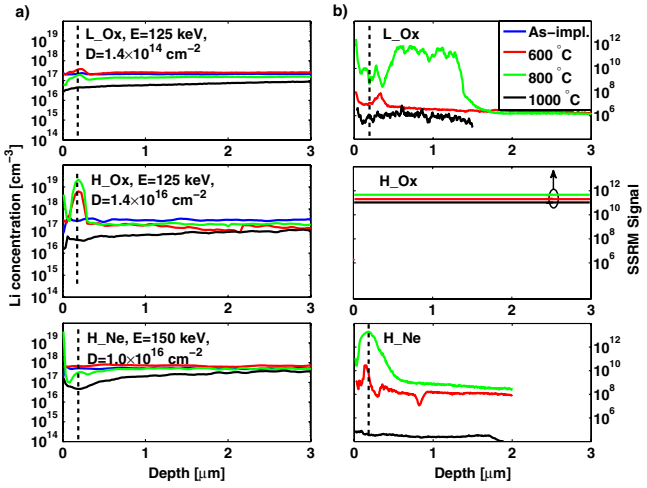

FIG. 2 (color online). (a) Li concentration versus depth profiles as measured by SIMS and (b) corresponding SSRM signals for O- and Ne-ion-implanted samples. The annealing time was 1 h for all the temperatures. The dashed lines indicate R_p of the implanted ions (~180 nm). The SSRM data for the H_Ox samples are above the range accessible by our setup.

indicate that the higher defect generation per incoming ion during Ar implants, relative to Ne implants, gives rise to more stable complexes of intrinsic acceptors, e.g., O_I- and/or V_{Zn}-related ones, but further investigations are required to confirm this speculation. For the H_Ox samples, the resistance remained above the maximum range of our setup, irrespective of the annealing temperatures used. This occurs in spite of nominally very similar primary defect production rates for the Ne and O ions, again leaving the surplus of implanted self-ions (O) as the most obvious explanation. More insight into the role of surplus O atoms is obtained by considering the resistance evolution in the L_Ox samples, Fig. 2(b). Between 600 to 800 °C, a region extending 1.4 μm beyond R_p converts from "low" to "high" resistance, without any significant Li redistribution. This suggests formation of intrinsic acceptor-like defects activated by the 800 °C anneal and O_I is a prime candidate. Further work is required for a quantitative determination of the defect reactions involved, but it is obvious that the amount of surplus (implanted) O ions is a decisive factor (and not the amount of displaced matrix atoms [and corresponding vacancies]).

This striking role of self-ion implantation on the point defect balance in ZnO, as demonstrated in Figs. 1 and 2, shows similarities with the so-called "+1 model" for Si, in which after a certain dose and annealing, the implanted self-ions occur as interstitials agglomorating into large cluster, eventually forming dislocation loops [18]. However, such a strong preferential annealing as observed in the present study is uncommon among most semiconductors; even for those with a high degree of ionicity and also for GaN, which is well-studied and behaves similar to ZnO with a strong dynamic annealing, such reports are scarce in the literature. On the other hand, one reason may be a lack of efficient means to monitor self-ions in GaN and metal oxide semiconductors, such as MgO, CdO, and CuO.

Figure 3 shows Li profiles after (a) isochronal and (b) isothermal annealing of H_Zn samples. The kick-out process starts at 600 °C and takes place in a relatively narrow region around R_p, Fig. 3(a), with a pileup after the depleted region (consistent with the data in Fig. 1(a)). The pile-up may be related to the electric field built up at the abrupt n^+-n-junction formed due to the Li redistribution; the field promotes rapid transport of the Li_I^+ donor from the n^+-region into the n-region where the transport slows down because it is now governed by thermal diffusion only. Hence, at sufficiently low temperatures where the diffusivity is low compared to the electric field effect, a pileup can be expected in the n-region. Further annealing gradually advances the depleted region reaching a maximum extension of ~8 μm after 750 °C. Then, at 775 °C a reverse process is initialized and Li starts to return to the depleted region, as indicated by indiffusion from the surface and an increased average concentration in the depleted region from $<1 \times 10^{14}$ to 8×10^{14} cm^{-3}. This increase

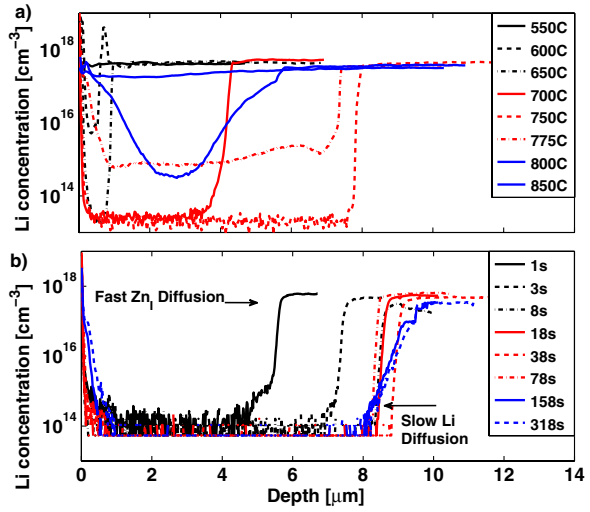

FIG. 3 (color online). Li concentration versus depth profiles as measured for (a) isochronal (30 min) and (b) isothermal (800 °C) anneals of H_Zn samples.

may be associated with a reestablishment of the equilibrium V_{Zn} concentration, after the source for injection of Zn_I is exhausted. These V_{Zn}'s are then able to capture Li_I's, rapidly moving into the depleted layer forming more stable Li_{Zn}'s. Annealing at 800 °C narrows the depleted region by diffusion from both the surface and the bulk. This process is much slower than the one yielding the depletion. Note some Li atoms always remain in the vicinity of the surface (even after the maximum depletion at 750 °C) and can contribute to the "refilling process." The presence of two Li diffusion mechanisms, as unveiled here, are in accordance with a fast transport of Li_I and a slow, vacancy-mediated one, of Li_{Zn} [16]. Annealing at 850 °C restores the Li content to the original bulk level throughout the sample and equilibrium conditions apply.

Figure 3(b) illustrates that the Zn_I's are released from the implanted region as a burst, and already after 1 s at 800 °C (heating rate 50 °C/s) Li is removed to a depth of 6 μm. With increasing duration, the depletion region becomes deeper reaching 8 μm after 78 s. The source of Zn_I's is then exhausted and the slow diffusion process controlling the refilling starts to dominate. In fact, this scenario complies with the +1 model for Si [18], discussed previously, and the associated transient-enhanced diffusion where a burst of self-interstitials promote rapid transport of dopants, like boron, via an interstitial-mediated process [19].

In conclusion, the role of excess intrinsic atoms for the residual point defect balance in ZnO has been discriminated by implanting Zn or O ions into Li-containing samples and monitoring the Li redistribution as well as the resistivity. Li-depleted regions with an extension of up to 8 μm occur beyond R_p in the Zn-implanted samples upon anneals at 600–800 °C, correlating with a decrease of the resistivity. In contrast, similar anneals of the O-implanted samples give rise to Li accumulation around R_p and a strongly increased resistivity. Based on comparison with Ar- and Ne-ion-implanted control samples, it is found that the surplus of implanted intrinsic atoms is decisive for the observed effects. The appearance of the Li-depleted regions is associated with excess of Zn_I's converting immobile Li_{Zn} to highly mobile Li_I. Correspondingly, the very high resistivity observed in the O-implanted samples, where no depletion of Li occurs, is associated with O_I-related acceptors compensating the native n-type doping. The diffusion of Li exhibits one fast and one slow process, presumably arising from interstitial-mediated (Li_I) and vacancy-mediated (Li_{Zn}) mechanisms, respectively.

The authors gratefully acknowledge financial support from the Norwegian Research Council through the NANOMAT, FRIENERGI, and FRINAT programs.

*neuvonen@phys.au.dk

[1] D. G. Thomas, J. Phys. Chem. Solids **15**, 86 (1960).
[2] D. C. Look, D. C. Reynolds, J. W. Hemsky, R. L. Jones, and J. R. Sizelove, Appl. Phys. Lett. **75**, 811 (1999).
[3] S. O. Kucheyev, P. N. K. Deenapanray, C. Jagadish, J. Williams, K. Yano, M. Koike, S. Sasa, M. Inoue, and K. Ogata, Appl. Phys. Lett. **81**, 3350 (2002).
[4] L. S. Vlasenko and G. D. Watkins, Phys. Rev. B **72**, 035203 (2005).
[5] S. O. Kucheyev, J. S. Williams, C. Jagadish, J. Zou, C. Evans, A. J. Nelson, and A. V. Hamza, Phys. Rev. B **67**, 094115 (2003).
[6] K. Maeda, M. Sato, I. Niikura, and T. Fukuda, Semicond. Sci. Technol. **20**, S49 (2005).
[7] B. G. Svensson, T. Moe Børseth, K. M. Johansen, T. Masqood, R. Schifano, U. Grossner, J. Christensen, L. Vines, P. Klason, Q. X. Zhao *et al.*, Mater. Res. Soc. Symp. Proc. **1035**, L04 (2008).
[8] L. Vines, E. V. Monakhov, R. Schifano, W. Mtangi, F. D. Auret, and B. G. Svensson, J. Appl. Phys. **107**, 103707 (2010).
[9] K. M. Johansen, A. Zubiaga, I. Makkonen, F. Tuomisto, P. T. Neuvonen, K. E. Knutsen, E. V. Monakhov, A. Yu. Kuznetsov, and B. G. Svensson, Phys. Rev. B **83**, 245208 (2011).
[10] C. H. Park, S. B. Zhang, and S.-H. Wei, Phys. Rev. B **66**, 073202 (2002).
[11] P. T. Neuvonen, L. Vines, A. Yu. Kuznetsov, B. G. Svensson, X. L. Du, F. Tuomisto, and A. Hallén, Appl. Phys. Lett. **95**, 242111 (2009).
[12] T. Moe Børseth, F. Tuomisto, J. S. Christensen, E. V. Monakhov, B. G. Svensson, and A. Yu. Kuznetsov, Phys. Rev. B **77**, 045204 (2008).
[13] Note the initial damage production when implanting self-elements and control elements is not fully identical because of the mass difference and subsequently different density of collision cascades, but it is still similar within a factor of less than two. Further, as shown in the present work, it is the amount of surplus self-interstitials surviving after annealing,

and not the ballistic generation of initial recoils, that directly matters for the observed redistribution of Li.

[14] J. P. Biersack and L. G. Haggmark, Nucl. Instrum. Methods **174**, 257 (1980).

[15] R. E. Williford, R. Devanathan, and W. J. Weber, Nucl. Instrum. Methods Phys. Res., Sect. B **141**, 94 (1998).

[16] A. Carvalho, A. Alkauskas, A. Pasquarello, A. K. Tagantsev, and N. Setter, Phys. Rev. B **80**, 195205 (2009).

[17] The Li redistribution around R_p in the H_Ar and H_Ne samples is similar to that in the L_Zn and H_Zn samples for the 600 °C anneals. This may indicate that the defects mediating the Li transport at this temperature originate from matrix recoils surviving recombination, while at 800 °C the interaction with surplus interstitials dominates.

[18] Y. Zhong, C. Bailat, R. S. Averback, S. K. Ghose, and I. K. Robinson, J. Appl. Phys. **96**, 1328 (2004).

[19] P. A. Stolk, H.-J. Gossmann, D. J. Eaglesham, D. C. Jacobson, C. S. Rafferty, G. H. Gilmer, M. Jaraíz, J. M. Poate, H. S. Luftman, and T. E. Haynes, J. Appl. Phys. **81**, 6031 (1997).